Sulfide Inclusions in Steel

L. K. BIGELOW AND M. C. FLEMINGS

New data on the Fe-Mn-S phase diagram are presented. One conclusion drawn using these data is that the rod-like "Type II" sulfides in steel result from eutectic solidification, not monotectic solidification. Effects of oxygen, carbon, silicon, and other elements on morphology of sulfides is shown experimentally. Oxygen leads to formation of Type I inclusions. Carbon and silicon reduce the solubility of sulfur in the melt and lead to various types of faceted sulfides including a faceted homologue of the rod-like Type II eutectic, and the "divorced" eutectic, Type III.

SULFIDE inclusions have long been a problem of major concern to steelmakers because inclusion morphology has a strong effect on ductility. Some types of interdendritic sulfides which are associated with the addition of a strong deoxidizer are particularly detrimental. However, deoxidation is frequently necessary to prevent the formation of blow-holes and porosity.

Much effort has been made to understand and control sulfide morphology. The work of Sims[1-7] is particularly well known. He proposed a system for classifying general morphological types which has persisted in the literature. He defined Type I as globular oxy-sulfides, Type II as the sheet-like or rod-like forms associated with deoxidation and reduced impact strength, and Type III as an angular form sometimes found in deoxidized melts. Dahl, Hengstenberg and Duren,[8] Mohla and Beech,[9,10] and others[11,12] have helped define the parameters which influence sulfide morphology. However, previous research into sulfide inclusion formation has generally been done in complicated alloy systems where isolation and control of all the variables is difficult, or has concentrated on a limited composition range. The present research eliminates some of these variables by starting with the simple Fe-Mn-S ternary system. The effects of controlled amounts of some added elements are then also studied. Deoxidation is accomplished either by a carbon boil or by the addition of aluminum. The effect of cooling rate on morphology is studied for a few composition ranges. Fracture surfaces from specimens containing representative examples of the different inclusion morphologies are examined with a scanning electron microscope.

EXPERIMENTAL PROCEDURE

The experimental alloys were made and solidified in a vacuum induction furnace, using high purity alumina crucibles. The ingots ranged in size from 50 to 500 grams. High purity materials, such as "Ferrovac-E" iron, were used throughout. Additions of master alloys containing manganese, carbon, and the other elements were made directly to the melt in the crucible, usually at 1650°C. During initial heating a vacuum of one-tenth of a micron was used. When the loss of volatile elements began to increase around 1200°C the furnace was backfilled with one-half an atmosphere of helium to minimize these losses. When a carbon-deoxidation was required, it was performed by pumping back down to 1000 microns to obtain a boil, then back-filling again during solidification. Various cooling rates from 0.1°C/s to 100°C/s were obtained by cooling with reduced induction power, by lifting the crucible out of the susceptor, or by touching the surface of the melt with a water cooled iron tube. Temperature was measured by means of a platinum-platinum/10 pct rhodium thermocouple which was protected by an alumina tube and inserted into the melt. Temperature was continuously monitored and recorded on a strip chart.

THE Fe-Mn-S PHASE DIAGRAM

The Fe-Mn-S system has been defined in the literature in its general outline, but there is disagreement on some details, and almost no firm data which can be used for quantitative studies.[13-18] The important portion of the phase diagram in the iron corner was investigated to provide more detailed information. The compositions of specimens used for the phase diagram and morphological studies are given in Tables I and II. Deoxidation of the melt was accomplished either by a carbon-boil, or by the addition of aluminum in order to determine whether changes in solidification behavior or sulfide morphology would result. No changes were observed.

Fig. 1 shows the liquidus isotherms in the iron corner of the Fe-Mn-S system. The isotherms were derived from the solidification curves of some of the

Table I. Fe-Mn-S System (Aluminum Deoxidized)

Alloy	Mn	S	O	Al(sol)	Al(insol)	O/S	Type	Liquidus Temp, °C
1*		0.10	0.009			0.09	IIS	
2	3.22	0.40					IIR, D, IP	1511
3	3.72	0.45					IIR, D, IP	1509
4	1.50	0.51	0.0046	0.053		0.009	IIR	
5	1.30	0.78	0.058	0.018	0.011	0.08	IIR, IIS	1486
6	3.18	0.82	0.0016	0.059		0.002	IIR, D, IP	1492
7	1.42	0.87	0.029	0.008	0.005	0.03	IIR, IIS, D	1480
8*	0.02	1.41	0.043	0.002	0.004	0.03	IIS	1481
9	2.81	0.72	0.0018	0.074			IIR, D	

*Aluminum was not added to these melts. However, since they do not properly fit into the Fe-Mn-S-O system or the carbon-deoxidized system they have been included here.

L. K. BIGELOW is Program Manager, Ledgemont Laboratory, Kennecott Copper Corp., Lexington, Mass. M. C. FLEMINGS is Abex Professor of Metallurgy, Department of Metallurgy and Materials Science, Massachussetts Institute of Technology, Cambridge, Mass. where L. K. Bigelow was formerly Research Assistant.

Manuscript submitted February 13, 1974.

Table II. Fe-Mn-S System (Carbon Deoxidized)

Alloy	Mn	S	O	C	Other	O/S	Type	Liquidus Temp, °C
10	4.51	0.37	0.0009	0.036		0.003	IIR, IP, D	
11	3.64	0.77	0.0018	0.084		0.002	IIR, IP	1496
12	1.13	0.42	0.0027	0.014		0.006	IIR	
13	2.03	0.78	0.0049	0.020		0.006	IIR, IP, D	1494
14	4.90	1.01	0.0029	0.023		0.003	IIR, IP, D	1490
15	2.76	1.18	0.013	0.027		0.011	IIR, IP, D	1490
16	2.07	1.22	0.0059	0.077		0.005	IIR, IP, D	
17	0.93	1.30	0.0041	0.0065	Al = 0.006	0.003	IIR, IIS, IP	
18	3.66	1.30	0.0042	0.078	P = 0.003	0.003	IIR, IP, D	
19	2.81	1.87	0.0027	0.054		0.001	IIR, D, IP	
20	0.00	1.83	0.0073	0.0026		0.004	IIS	
21	0.63	2.62	0.011	0.042		0.004	IIS, IIR, IP	

Table III. Fe-Mn-S-O System

Alloy	Mn	S	O	Al(sol)	Al(insol)	O/S	Type	Liquidus Temp, °C
22			0.17				I	
23	0.12	0.07	0.01			0.14	I	
24	0.12	0.07	0.01			0.14	I	
25	0.52	0.20	0.029			0.14	I, IIs	
26		0.67	0.20			0.29	IIS, I	
27	0.56	1.56	0.033	0.006	0.009	0.02	IIS, I	1466
28	0.32	1.63	0.069	0.002	0.001	0.04	I, IIS	1468
29	1.89	1.10	0.10			0.09	IIR, IIS, I	
30		2.78	0.21			0.075	IIS, I	
31		8.22	0.40			0.05	IIS, I	

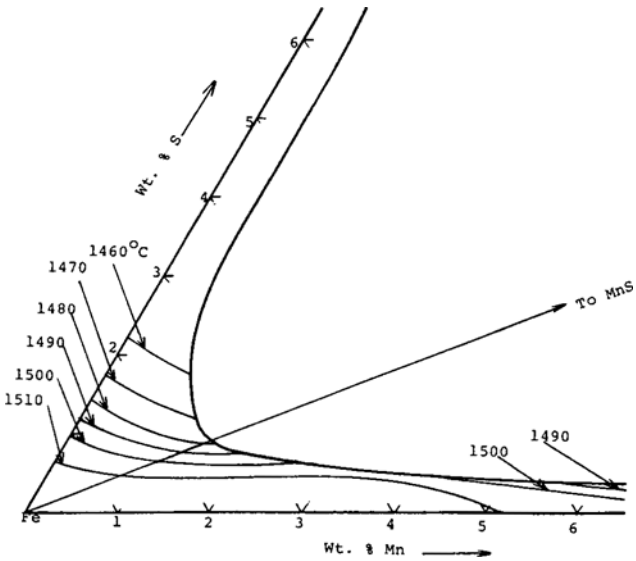

Fig. 1—Liquidus isotherms and eutectic in iron corner of Fe-Mn-S system.

specimens, as listed in Tables I, II, and III. The temperature at which thermal arrest occurred upon cooling was taken as the liquidus temperature. Although three of the data points were taken from the Fe-Mn-S-O system (Table III) the oxygen levels were low enough so that the error from the impurity oxygen should be 5°C or less. The eutectic valley rises to a maximum near 1510°C. It remains roughly on a plateau in the composition range 3-5 pct Mn, 0.5 pct S, but falls rapidly toward the Fe-S binary side and slowly in the direction parallel to the Fe-Mn binary.

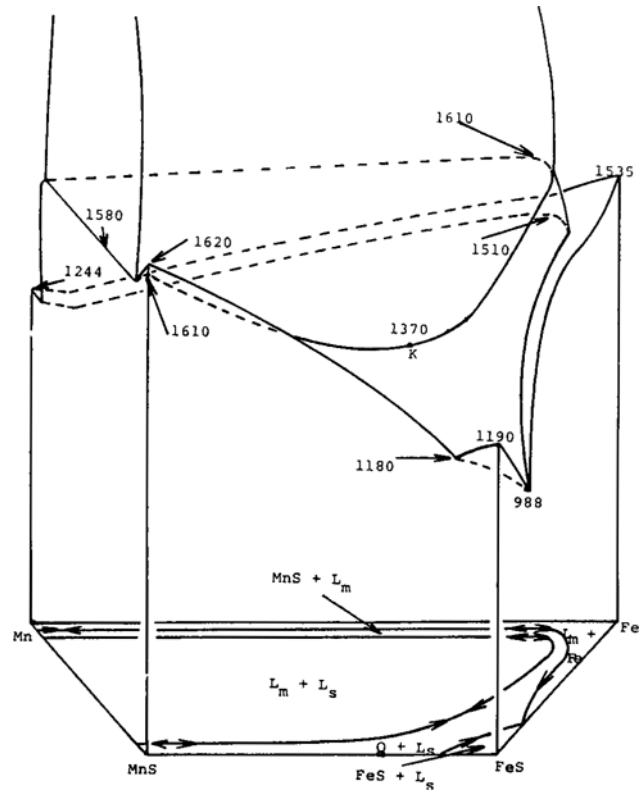

Fig. 2—Appearance of Fe-Mn-S ternary, qualitatively represented. Temperatures in °C.

A qualitative representation of a portion of the Fe-Mn-S phase diagram is shown in Fig. 2, which has been distorted to show the features more clearly. The temperatures represent the authors' best judgement of the correct values from previous research,[13-18] as supported or modified by our own observations and experiments. The observed precipitation and growth behavior of the sulfides is consistent with the temperature values and phase boundaries shown on Fig. 2. The diagram, for example, agrees with Vogel,[16] but not with Schurmann,[17] in that the miscibility gap does not intersect the eutectic valley on the Fe-FeS side,[19] because the sulfide morphologies which were found in that region were not consistent with Schurmann's version.

SULFIDE MORPHOLOGY IN THE Fe-Mn-S SYSTEM

Sulfide morphology in this system was investigated by adding manganese to a sulfur-bearing melt at various temperatures, followed by solidification over a range of rates. Fig. 3 is a qualitative projection of the Fe-Mn-S diagram showing the important features, and is divided for discussion purposes into six regions by the stoichiometric MnS line and eutectic and monotectic boundaries.

When sufficient manganese is added to a sulfur-bearing melt heated to 1650°C so that the melt composition falls into Region A, within the miscibility gap, three types of sulfide inclusion are formed on subsequent cooling: spherical MnS particles with included iron, MnS dendrites, and rod-like inclusions which are of the type usually categorized as Type II, and are here designated Type IIR (Fig. 4). These

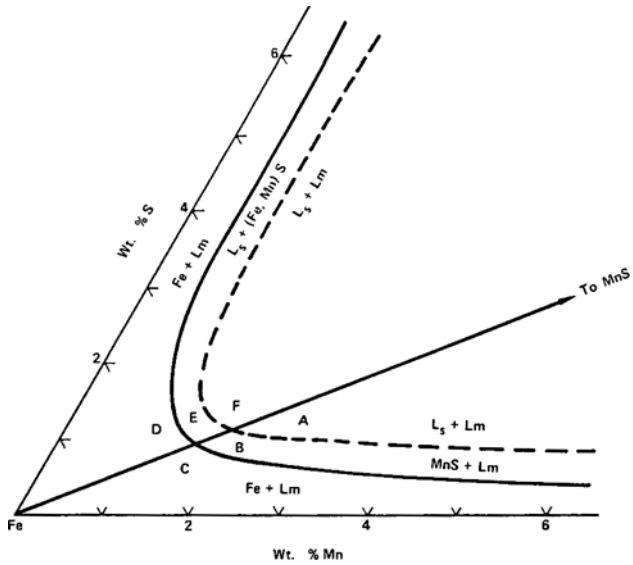

Fig. 3—Qualitative projection of Fe-Mn-S systems, divided into six composition regions for purposes of discussion.

Fig. 4—Alloy 18, from Table II. 3.7 pct Mn, 1.3 pct S, Magnification 240 times.

morphologies can be explained as follows: When the manganese is added, liquid slag droplets form and float toward the surface. When the melt temperature falls to the monotectic $L_M + L_S \rightarrow L_M + L_S$ + MnS (solid) in the range 1610 to 1580°C, and the slag droplets freeze, while rejecting small amounts of iron. As the droplet solidifies it shrinks, with resultant intrusion of the liquid iron, Fig. 5. These round inclusions are different from Sims' conventional Type I inclusions and are here designated Type IP because they are a primary phase. They occur in deoxidized melts with an excess of sulfur and manganese. Below the monotectic, sulfide dendrites nucleate and grow into the melt as the temperature falls toward the eutectic valley. As the temperature drops below the eutectic, at 1510°C or less, iron dendrites are nucleated while manganese sulfide continues to precipitate on the preexisting solid sulfide slag particles and dendrites. Cooperative growth subsequently occurs, with the resulting rod eutectic comprising the remainder of the structure, (Fig. 4).

Fig. 5—Alloy 6, Table I. Detail of typical large Type I MnS inclusion, showing intrusion of liquid iron on solidification of droplet, 3.18 pct Mn, 0.82 pct S, Magnification 600 times.

If the composition falls exactly on the eutectic so that preexisting solid sulfide is absent, then the structure consists of 100 pct eutectic (Fig. 6). Fredriksson and Hillert[20] recently concluded that the rod-like inclusions are the result of a monotectic reaction, not of entectic solidification, and Baker and Charles[21] have also considered this possibility. However, the melting point of MnS, while not specifically measured in this research, was observed to be well above the melting point of iron, not in the 1530°C range assumed by Fredriksson and Hillert.[14] Manganese sulfide dendrites frequently extend across and through several neighboring iron dendrite arms (Figs. 4 and 7). This is clearly possible only if the sulfide solidified first and was later surrounded by the iron dendrites (Figs. 4 and 7). In the specimen shown in Fig. 7 the manganese was added at a temperature (1547°C) well above the freezing point of iron and in the composition region A. Excess MnS beyond the liquid solubility limit immediately separated as MnS dendrites. The primary type IP slag droplets were not formed, since the temperature was below the freezing point of the sulfide. Since the sulfide is solid above the melting point of iron, rod formation in this specimen and similar de-oxidized specimens must be by eutectic solidification.

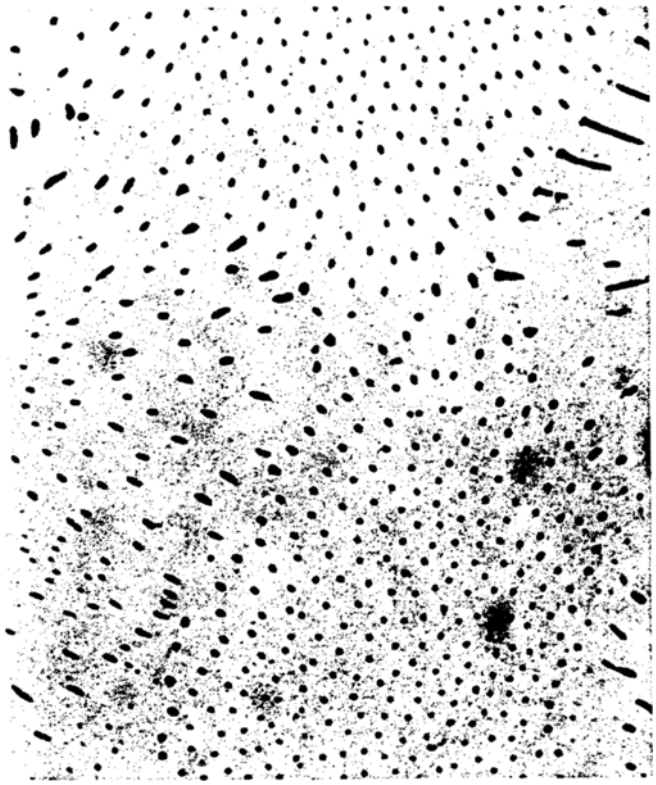

Fig. 6—Alloy 15. Rod eutectic. 2.76 pct Mn, 1.18 pct S, Magnification 240 times.

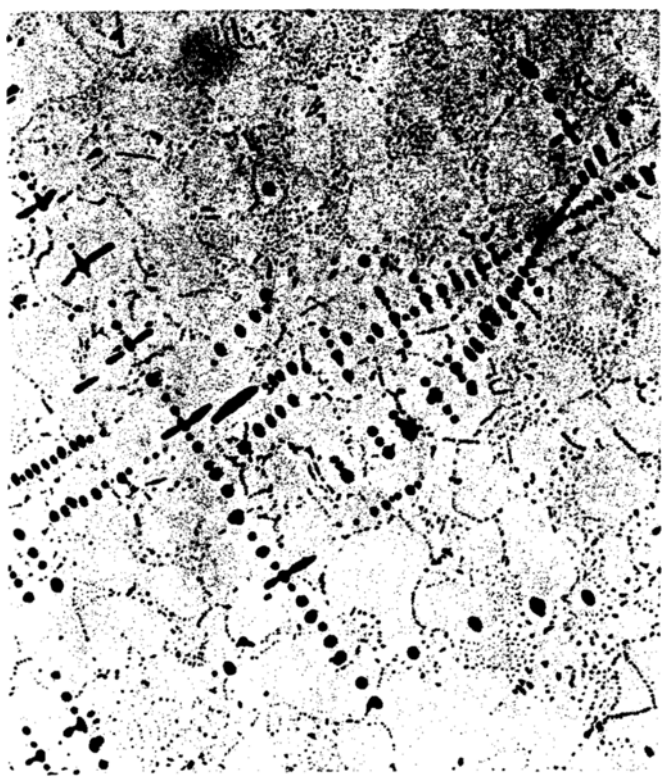

Fig. 7—Alloy 9. Extensive sulfide dendrites, together with Type IIR, formed when manganese is added to a melt at 1547°C, below the freezing temperature of MnS, to put the overall composition in the L + MnS region. 2.81 pct Mn, 0.72 pct S, Magnification 120 times.

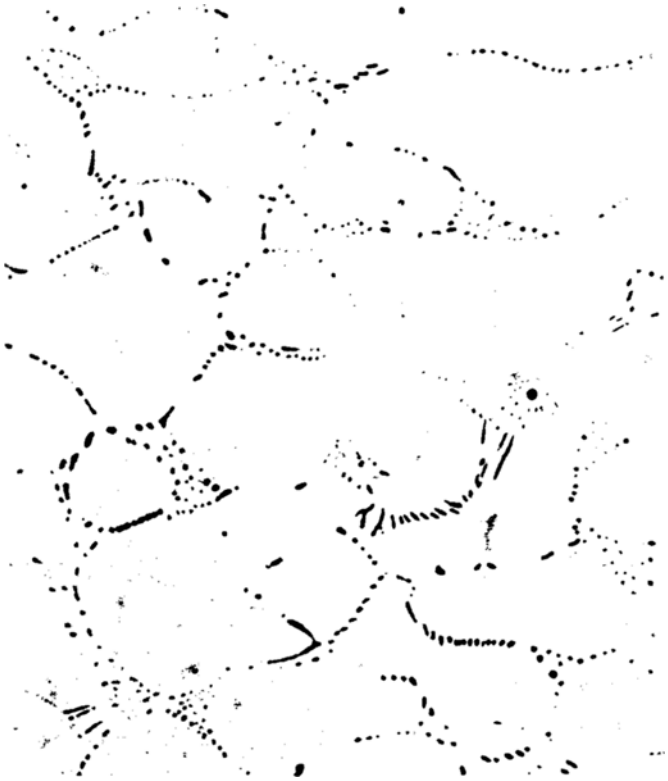

Fig. 8—Alloy 17. Composition initially in Fe and L_m region on manganese-rich side of phase diagram. 1.13 pct Mn, 0.42 pct S, Magnification 300 times.

Fig. 9—Alloy 12. Degenerate rod morphology. 0.93 pct Mn, 1.3 pct S, Magnification 600 times.

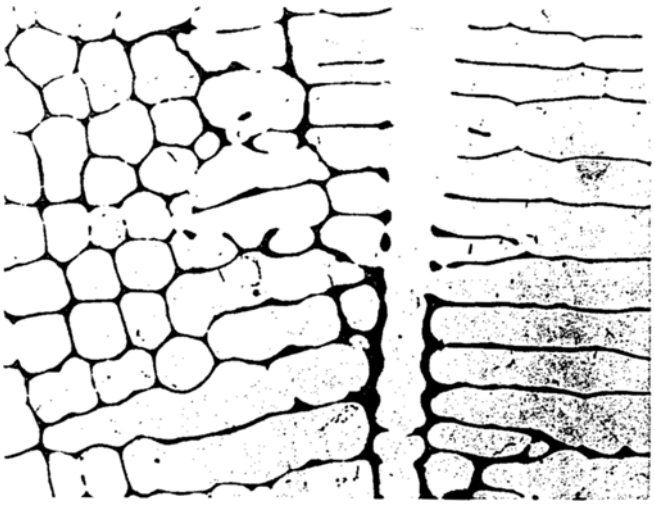

Fig. 10—Alloy 20. Sheet-like Type IIS sulfide formed at high sulfur level in the absence of manganese. 0 pct Mn, 1.83 pct S, Magnification 88 times.

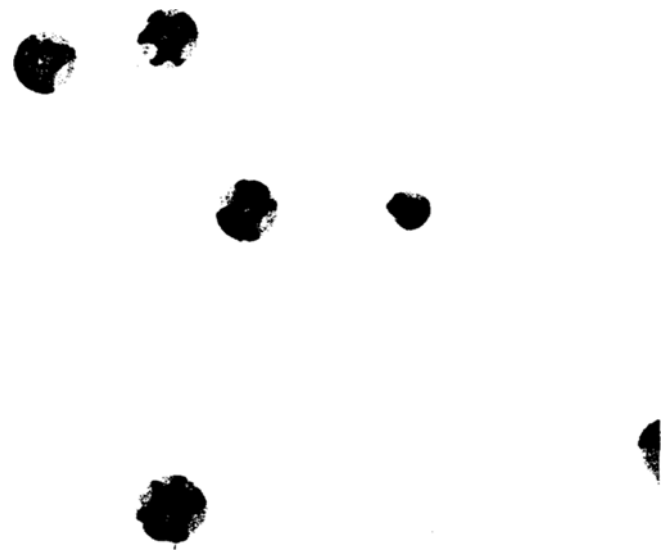

Fig. 11—Alloy 23. Duplex Type I inclusions of MnO and MnS. 0.12 pct Mn, 0.07 pct S, 0.01 pct O, Magnification 1200 times.

Solidification of compositions in Region C leads to the precipitation of primary iron dendrites followed by interdendritic rod eutectic (Fig. 8). On the other hand, if there is an initial excess of sulfur over manganese (Region D) or if the different segregation ratios of these elements during solidification creates an excess in the remaining liquid, then a duplex MnS-FeS sulfide results. This sulfide can have a degenerate rod form (Fig. 9), but transforms into the sheet-like form we designate Type IIS as the Mn/S ratio is decreased (Fig. 10).

Type III inclusions were not found in the deoxidized

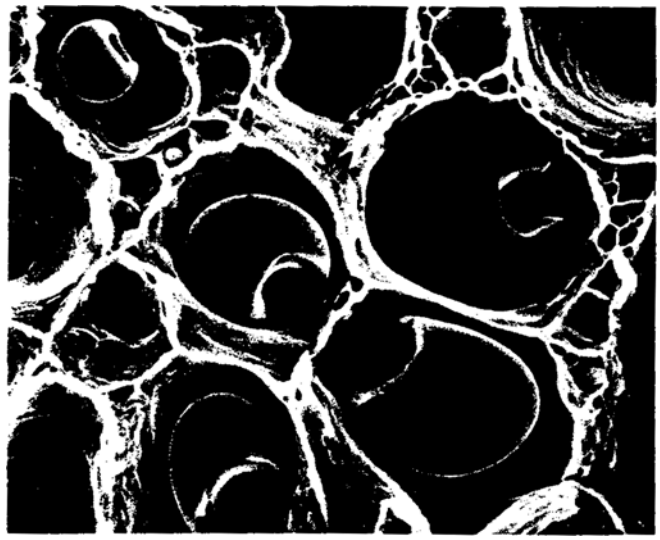

Fig. 12—Scanning electron microscope picture of Type I inclusions in Alloy 25. 0.52 pct Mn, 0.20 pct S, 0.029 pct O, Magnification 1600 times.

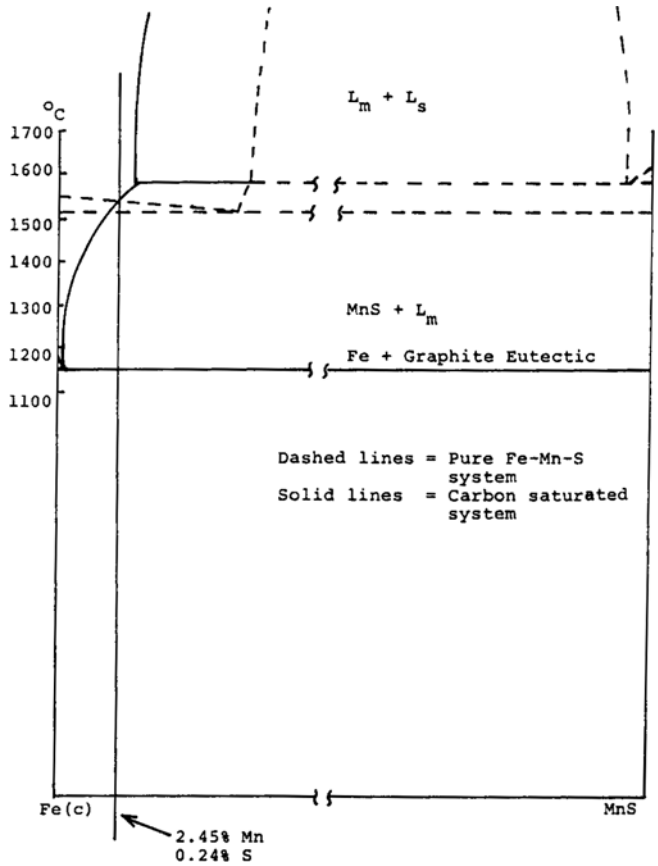

Fig. 13—Pseudo-binary cuts between Fe and MnS for pure system (dashed lines), and for carbon saturated system. Shows that an initial composition of 2.45 pct Mn and 0.24 pct S would intersect Fe + L_m region in the former, and MnS + L_m region in the latter.

Fe-Mn-S system, even when a substantial excess of aluminum was present, as in some alloys in Table I. Deoxidation by a carbon boil, provided the residual amount of carbon is small, is likewise incapable of producing Type III inclusions. These results are consistent with the findings of Dahl, Hengstenberg, and Duren.[8]

SULFIDE MORPHOLOGY IN THE Fe-Mn-S-O SYSTEM

Little experimental information is available on this system although Hilty and Crafts[18] explored certain features of it, and presented a qualitative section of the phase diagram which is apparently incorrect in certain features.[19] A few experimental melts were made in this system, (Table III).

Type I inclusions form in commercial alloys as secondary inclusions during growth of iron dendrites when segregation of oxygen and sulfur into the interdendritic spaces reaches a sufficiently high level, (Fig. 11). The droplets are entrapped by the growing dendrites[22] and eventually freeze after the metal, resulting in shrinkage dimples (Fig. 12). When slag droplets are formed in this manner by secondary precipitation in commercial compositions, Type IIR and IIS inclusions are generally not found. However, at higher levels of sulfur (Alloys 25-31) the sheetlike morphology can coexist with Type I. At these composition levels, the miscibility gap is intersected earlier in solidification resulting in the formation of droplets which are often found entrapped within dendrite arms. In the case of the pure Fe-S-O system[22] a plait point is reached as solidification proceeds, followed finally by the formation of Type IIS inclusions. Similar behavior is observed in the present system which is modified by manganese, except that at higher manganese levels (Alloy 29) some of the rod eutectic also precipitates.

SULFIDE MORPHOLOGY IN Fe-Mn-S ALLOYS WITH C AND Si

Angular or faceted sulfides (Type III) occurring in deoxidized commercial alloys result from the segregation of manganese and sulfur together with elements such as carbon and silicon which decrease sulfur solubility and extend the liquid state to lower temperatures. The pronounced effect of carbon can be seen in Fig. 13. This figure was derived from the work of Schurmann,[17] Fig. 14, on the equilibrium of manganese and sulfur in iron which is melted in a graphite crucible and is therefore saturated with carbon. Schurmann's diagram is not a true ternary diagram nor equivalent to a series of sections through the Fe-Mn-S-C quaternary since the carbon content is not constant, but is nevertheless a useful construction for illustrating the effect of carbon on sulfur solubility. If a vertical plane is erected which passes through 2.45 pct Mn, 0.24 pct S (Alloy 34) and MnS in Fig. 14 it would intersect the phase boundaries as shown in Fig. 13 by the solid lines. For comparison, a similar plane through the Fe-Mn-S ternary would generate the dashed lines. The important differences are the lowering of the eutectic temperature and the great reduction in sulfur solubility at the eutectic. The vertical line shows that Alloy 34 would precipitate iron as the primary solid phase in the absence of carbon, but that near carbon saturation the primary solid phase becomes the sulfide. The temperature range over which solid sulfide can precipitate at this composition is more than 300°C greater than in the basic Fe-Mn-S system. The solubility limit for sulfur in Alloy 34 should be reached between 1500°C and 1550°C at which point dendrites of MnS will begin to grow in the melt. Type III

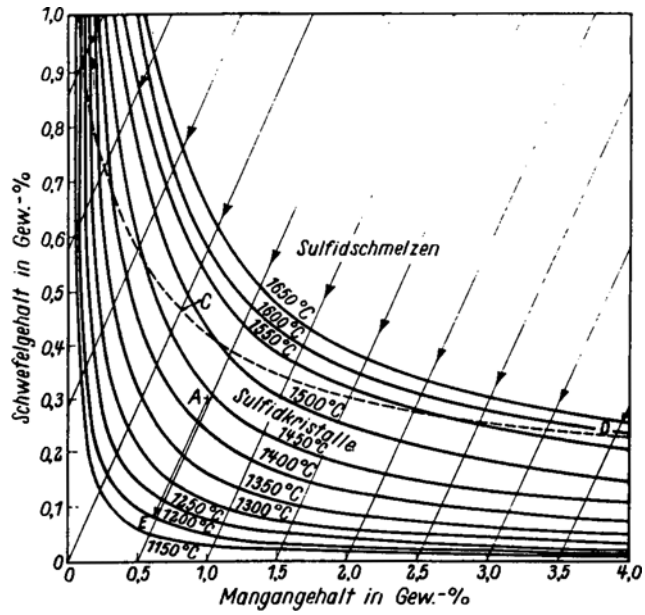

Fig. 14—Derived from Schurmann.[17] Shows sulfur solubility as a function of temperature and manganese content for iron melted in a graphite crucible. Dashed curved line is the boundary between the miscibility gap and region of solid sulfide formation. If initial melt composition falls on one of the diagonal parallel lines, subsequent melt composition follows the same line as temperature decreases.

Fig. 15—Type III inclusions in Alloy 34. 2.45 pct Mn, 0.24 pct S, 4.43 pct C, Magnification 600 times.

inclusions were also found at these levels of carbon, sulfur, and manganese in Alloys 34 to 36. Examples of the morphologies observed are shown in Figs. 15 to 17. Precipitation of sulfides may reduce the sulfur level in the liquid prior to the start of freezing of the

Table IV. Fe-Mn-S-C System

Alloy	Mn	S	C	O	O/S	Type
32	0.83	0.07	3.43	0.003	0.04	III
33	2.63	0.15	1.76			III
34	2.45	0.24	4.43			III, D
35	2.60	0.65	3.66			III, D, IP
36	2.64	0.66	3.01			IIF, D, IP

Table V. Fe-Mn-S-Si System

Alloy	Mn	S	Si	C	O	O/S	Type
37	0.89	0.036	7.97		0.006	0.16	III
38	0.94	0.05	7.97		0.010	0.20	III, IIF
39	2.02	0.09	7.60				III
40	1.91	0.11	8.03				III, IIF
41	2.62	0.10	8.61				III, IIF
42	2.73	0.41	7.41				D, IP
43	2.04	0.44	7.49	0.063	0.003	0.008	D, III, IP, IIF
44	3.46	0.49	7.71				D, IP
45	2.08	0.58	6.76	0.073	0.002	0.004	D, IP
46	2.01	0.73	8.07				D, III, IIF
47	2.58	0.16	7.43		0.018	0.1	IP, IIF
	P = 0.004						

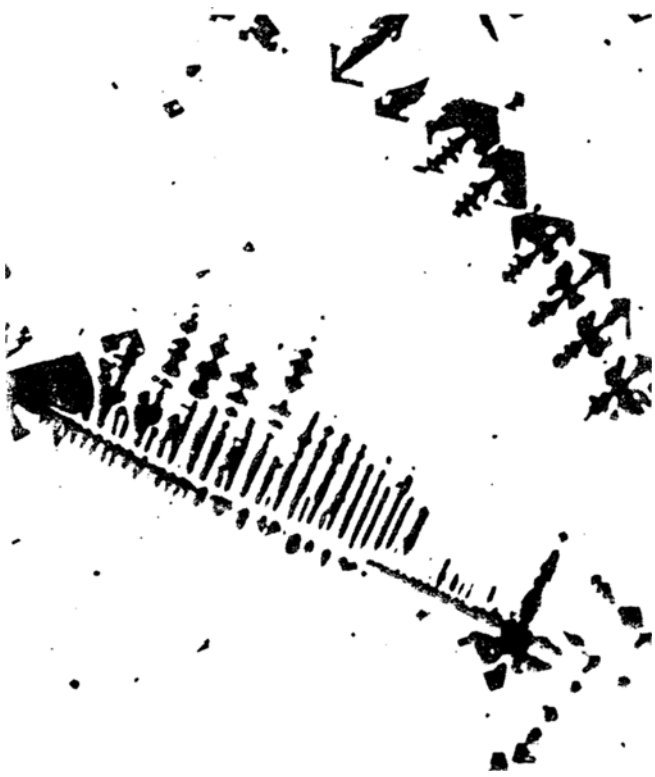

Fig. 16—Faceted dendrite in Alloy 35. 2.6 pct Mn, 0.65 pct S, 3.66 pct C, Magnification 120 times.

iron to as low as 0.02 pct, with a final solidification temperature as low as 1150°C. As a result of the dilute solution and low temperature, interface kinetics are sufficiently slow that growth is faceted, as has been observed in other similar instances.[23,24] Identical forms are observed in high silicon systems (Table V).

Flotation of Type III inclusions and a few coarse

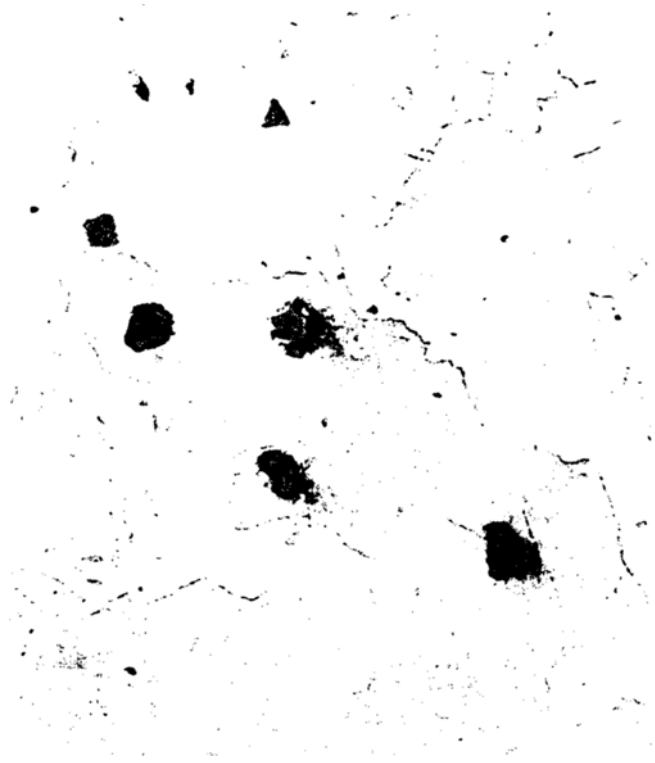

Fig. 17—Alloy 35. Random location of Type III inclusions with respect to iron dendrites and Fe-Fe_3C eutectic. 2.60 pct Mn, 0.65 pct S, 3.66 pct C, Magnification 240 times.

Table VI. Fe-Mn-S-Si-C System

Alloy	Mn	S	C	Si	O	O/S	Al(sol)	Type
48	0.59	0.06	0.45	0.46			<0.03	III, IIR
49	0.56	0.06	0.41	0.47			0.03	III, IIR
50	2.70	0.15	1.56	2.10	0.002	0.013		III, IIF
51	0.59	1.16	0.20	2.15	0.005		0.004	IIR, IP, D

dendritic structures was observed in Alloys 34 to 36, indicating that they are alternate morphologies of the primary phase. Baker and Charles[21] did not observe the formation of primary Type III inclusions because the carbon levels of their experimental alloys were too low. However, the high levels of carbon and silicon discussed above will rarely occur in commercial practice except in interdendritic regions, and so Type III inclusions usually form as an angular "divorced" eutectic which replaces the rod eutectic formed in less highly alloyed specimens. In borderline cases where the carbon and silicon levels are relatively low it is possible to have both faceted and rod morphologies (Table VI, Figs. 18 and 19). At composition levels like that of Alloys 48 and 49, Sims[4] found that increasing amounts of aluminum favored a gradual transition from Type IIR to Type III. Whereas aluminum is incapable alone of causing Type III inclusions to form, it evidently can promote the transition in borderline cases through a modification of the kinetics or phase relations which has not been determined.

Another morphology found in systems containing carbon and/or silicon is a script-like form designated

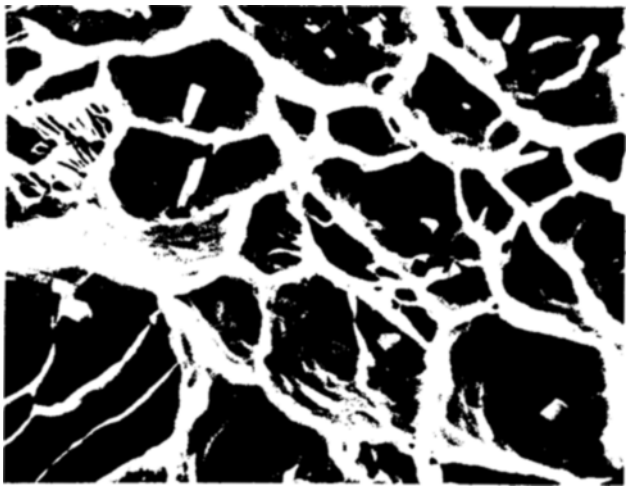

Fig. 18—Scanning electron microscope picture of fracture surface of Alloy 49 showing coexistence of angular Type III inclusions with rod-like inclusion. 0.56 pct Mn, 0.06 pct S, 0.41 pct C, 0.47 pct Si, Magnification approx. 2433 times.

Fig. 19—Dominant Type IIR inclusions in fracture surface of Alloy 49. Scanning electron microscope picture. Magnification 1560 times.

here Type IIF (Fig. 20). It apparently can be nucleated and grow from pre-existing sulfide dendrites (Fig. 21). The Type IIF morphology can coexist with Type III, but the formation of Type IIF was found to be favored by increasing the cooling rate, in confirmation of the results of Mohla and Beech.[9,10] Alloys 37 and 39 (Table V) and 35 (Table IV) were cooled at rates of about 1°C/s and produced only Type III inclusions whereas rapidly solidified Alloys 38, 40 and 46 contained a large fraction of Type IIF, especially near the water-cooled chill tube which was immersed in the melt. The script morphology is a faceted-non-faceted eutectic similar to that found in many other systems. It grows cooperatively as does the eutectic Type IIR morphology, not in divorced fashion as does the eutectic Type III. Fig. 22 shows that the Type IIF inclu-

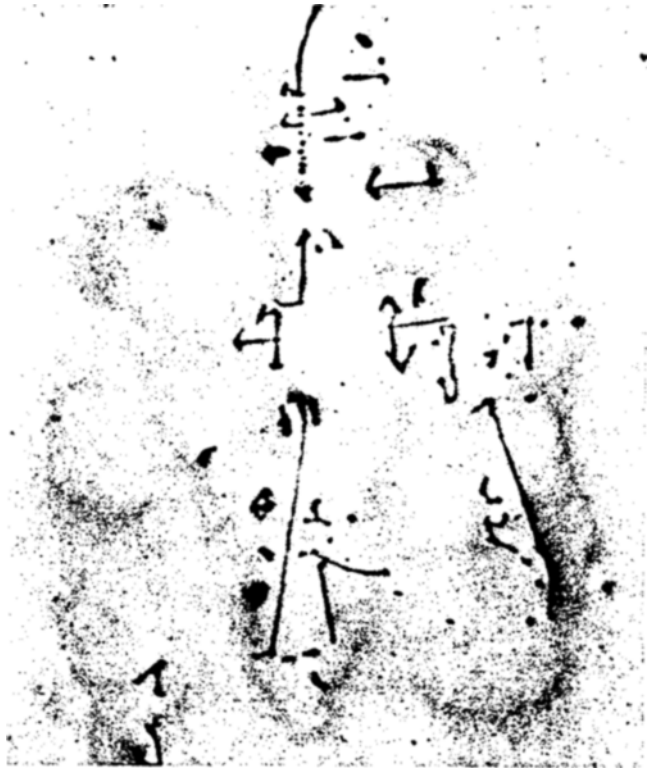

Fig. 20—Alloy 36. Script-like Type IIF morphology, also observed in Fe-Mn-S system. 2.64 pct Mn, 0.66 S, 3.01 pct C, Magnification 240 times.

Fig. 21—Alloy 36. Type IIF morphology growing from faceted dendritic sulfide. Magnification 240 times.

Fig. 22—Association of Type IIF inclusions with the iron dendrites which form prior to the Fe-Fe_3C eutectic. Alloy 36. 2.64 pct Mn, 0.66 pct S, 3.01 pct C, Magnification 120 times.

sions are formed together with extensions or protrusions off the original γ-dendrites. By contrast, Type III inclusions are found both entrapped within the dendrite arms and in the interdendritic spaces (Fig. 17).

CONCLUSIONS

1) New data on the Fe-Mn-S phase diagram in the iron corner has been generated and presented. Solidification in various composition regions is studied and the resulting morphologies are explained. One conclusion is that the rod-like sulfide inclusions found in deoxidized melts result from eutectic solidification, not monotectic solidification.

2) The Fe-Mn-S-O system was studied. The precipitation and entrapment as a liquid of Type I inclusions is discussed.

3) The effects of carbon, silicon, and other elements which reduce the solubility of sulfur in the melt are considered. The morphologies which result are primarily the result of growth from a dilute solution. A script-like morphology, here designated Type IIF, is a faceted dilute solution homologue of the rod-like eutectic (Type IIR). Its formation is favored over the "divorced" angular Type III form also found in dilute solutions by increased cooling rates. Evidence is presented that Type III sulfides can be the primary solid phase, but only in a limited composition range not found in commercial compositions. All three morphologies are eutectics when found in deoxidized commercial alloys. The appearance of a particular one of these three morphologies is governed primarily by melt composition and cooling rate.

ACKNOWLEDGMENTS

This work was sponsored by Army Materials and Mechanics Research Center, Watertown, Massachusetts.

REFERENCES

1. C. E. Sims and G. A. Lillieqvist: *Trans. AIME*, 1932, vol. 100, p. 154.
2. C. E. Sims and F. B. Dahle: *Trans. Amer. Foundrymen's Assoc.*, 1938, vol. 46, pp. 65-104.
3. C. E. Sims, H. Saller, and F. Boulger: *Trans. Amer. Foundrymen's Soc.*, 1949, vol. 57, p. 233.
4. C. E. Sims, H. Saller, and F. Boulger: *Trans. AIME*, 1949, vol. 185, p. 814.
5. C. E. Sims: *AIME Elec. Furn. Proc.*, 1952, vol. 10, pp. 152-71.
6. C. E. Sims: *Trans. TMS-AIME*, 1959, vol. 215, pp. 367-93.
7. C. E. Sims and C. Briggs: *AIME Elec. Furn. Proc.*, 1959.
8. W. Dahl, H. Hengstenberg, and C. Düren: *Stahl Eisen.*, 1966, vol. 86, no. 13, pp. 782-95. (Brutcher Translation H.B. No. 6928).
9. P. P. Mohla and J. Beech: *Brit. Foundryman*, Dec. 1968, pp. 453-60.
10. P. P. Mohla and J. Beech: *J. Iron Steel Inst.*, 1969, vol. 207, pp. 177-80.
11. A. Gagnebin: *Trans. Amer. Foundrymen's Assoc.*, 1938, vol. 46, pp. 133-55.
12. W. J. Lichy, G. C. Duderstadt, and N. J. Samways: *J. Metals*, 1965, vol. 17, no. 7, pp. 769-75.
13. O. Meyer and F. Schulte: *Arch. Eisenhuettenw.*, 1934-1935, vol. 8, pp. 187-95.
14. F. Körber and W. Oelsen: *Stahl Eisen*, 1936, vol. 56, pp. 441-44.
15. H. Wentrup: *Tech. Mitt. Krupp*, 1937, vol. 5, pp. 131-52.
16. R. Vogel and W. Hotop: *Arch. Eisenhuettenw.*, 1937, vol. 11, pp. 41-54. (Brutcher Translation H.B. No. 459).
17. E. Schurmann, *Giesserei*, 1961, vol. 48, pp. 481-87.
18. D. C. Hilty and W. Crafts: *Trans. AIME*, 1954, vol. 200, pp. 959-68.
19. L. K. Bigelow: Massachusetts Institute of Technology, Metallurgy Department, Ph.D. Thesis, 1970.
20. H. Fredriksson and M. Hillert: *J. Iron Steel Inst.*, 1971, vol. 209, p. 109.
21. T. J. Baker and J. A. Charles: *J. Iron Steel Inst.*, 1972, vol. 210, pp. 702-06.
22. J. Yarwood, M. C. Flemings, and J. F. Elliott: *Met. Trans.*, 1971, vol. 2, pp. 2573-82.
23. W. A. Miller and G. A. Chadwick: *J. Iron Steel Inst.*, 1968, Publication 110, pp. 49-56.
24. D. Saratovkin: *Dendrite Crystallization*, translated by Consultants Bureau, Inc., New York, 1959.